Application of the layer Korringa-Kohn-Rostoker method to the calculation of near-edge structure in x-ray-absorption and electron-energy-loss spectroscopy

Peter Rez
Department of Physics and Astronomy and Center for Solid State Science, Arizona State University, Tempe, Arizona 85287-1704

James M. MacLaren
Department of Physics, Tulane University, New Orleans, Louisiana 70118

Dilano K. Saldin
Department of Physics and Laboratory for Surface Studies, University of Wisconsin–Milwaukee, P.O. Box 413, Milwaukee, Wisconsin 53201

(Received 22 July 1997)

Green's-function methods are frequently used in the calculation of both the extended and the near-edge structures observed in x-ray-absorption and electron-energy-loss spectroscopies. To date, calculations based upon these methods have tended to be based upon a superposition of atomic potentials used to represent the crystal potential, with no attempt to calculate the self-consistent electronic potential. Many features in the near-edge region relate to charge redistribution and therefore are only approximately described by non-self-consistent electronic potentials. In this paper we show that the layer Korringa-Kohn-Rostoker method can be used in the same way as conventional Green's-function theories for near-edge structure, with the added advantage that the self-consistent ground-state charge is used. Spectra calculated in this manner, and compared with those obtained from other Green's-function methods, demonstrate that self-consistency is necessary to show certain features such as molecular orbital splitting in TiO_2 (rutile). [S0163-1829(98)10903-7]

INTRODUCTION

Near-edge structure (NES), observed in x-ray-absorption or electron-energy-loss spectroscopy of inner-shell ionization processes, can be sensitive to interatomic distances, local coordination, and local electronic structure. The analysis of near-edge structures can be particularly valuable as the excitation is specific to a given atomic species and can be localized in a nanometer-sized region in scanning transmission electron microscopy. To understand the origins of various features it is necessary to calculate the observed fine structures from a suitable theoretical model. This process is an essential first step before the fine structure can be used to investigate problems of local structural and electronic changes for atoms in a different environment. The extended fine structure, which is much weaker than the NES, can be easily analyzed on the basis of the single-scattering extended x-ray-absorption fine-structure (EXAFS) theory.[1] In this model the outgoing spherical wave representing the ejected electron is partially reflected back from neighboring atoms. The resulting interference leads to sinusoidal oscillations in the fine structure as a function of ejected electron wave vector. Mathematically, the process is best represented by Green's functions for the partial waves of different angular momentum. The scattering by the atoms is then represented by phase shifts. The model can be extended by allowing multiple scattering of the electron between the atoms. This idea forms the basis of many of the techniques for calculating near-edge structure, the differences being mainly in the way that scattering paths are selected. In the x-ray-absorption near-edge structure (XANES) method[2,3] the neighboring atoms are assigned to shells around the excited atom. Various combinations of scattering events within a given coordination shell (intrashell) and scattering between different shells (intershell) can be considered. Fujikawa, Matsuura, and Kuroda[4,5] have also published a multiple-scattering theory where no explicit path selection technique is used and presented results of calculations. The *f* effective (FEFF) method[6] was developed as a direct extension of EXAFS theory and selects scattering paths according to a maximum path length cutoff, the number of scattering events, and the estimated amplitude. Natoli *et al.*[7,8] have published a generalization of the multiple-scattering theory that allows for multiple excitation channels. In all these theories, with the notable exception of the related X_α method for molecular clusters, a superposition of atomic potentials is used[9] and no attempt is made to calculate the ground-state charge density. This might not be so important in the EXAFS region beyond 100 eV above the edge threshold, but it might lead to serious errors in the near-edge region within the first 10–20 eV. Although a multiple-scattering calculation, such as one performed by a XANES program,[2,3] has been used to calculate features in a near-edge spectrum due to electronic transitions to unoccupied antibonding orbitals in simple diatomic molecules,[10] fully self-consistent calculations of the potential are necessary to model the precise energies and shapes of the spectral peaks in more complex systems.

Near-edge structure can also be viewed as the appropriate angular-momentum-resolved unoccupied density of states at the excitation site.[11,12] For example, a *K*-shell excitation probes the unoccupied *p* states and an L_{23} excitation probes unoccupied *s* and *d* states. Accordingly, the features in a spectrum can be interpreted using a appropriate electronic-structure calculation technique that can produce site-specific,

angular-momentum-resolved, conduction-band densities of states. Those methods that rely on muffin-tin descriptions of the atomic core region, such as the augmented plane-wave (APW) method[13] and the Korringa-Kohn-Rostoker (KKR) method,[14,15] and derivatives such as the layer KKR (LKKR) approach,[16,17] can give the desired result directly. For plane-wave pseudopotential methods the appropriate densities of states can be obtained by projection from the plane-wave states.[12] Whichever method is used, the ground-state charge density is calculated self-consistently using density-functional theory. Exchange and correlation are treated in the local-spin-density approximation. This contrasts with the usual multiple-scattering methods used to interpret experimental spectra, in which no attempt is made to solve for a self-consistent charge density, although the latest schemes do incorporate energy-dependent exchange-correlation potentials.[18,19] While in principle all of these cluster-based methods can either be made self-consistent or use self-consistent potentials derived from other electronic-structure methods, in practice overlapped atomic charge densities are used to construct the crystalline potential. The LKKR method provides a convenient method for computing the charge density and the near-edge structure spectra within the same methodology. It is important to remember that in band-structure methods the wave function satisfies a Bloch condition appropriate for an infinite solid, while the usual multiple-scattering models assume a cluster of atoms around the excited atom. Possible core-hole effects are therefore readily incorporated into the multiple-scattering theories, but are more difficult to consider in most band-structure codes. Actually, the Green's-function-based KKR and LKKR codes can handle the self-consistent embedding of an impurity in an otherwise perfect host crystal.[20]

The KKR method is based on the division of the crystal into muffin tins within which spherical potentials are assumed. Green's-function expansions, as used in the cluster multiple-scattering theories, are used to treat interatomic multiple-scattering events. In the KKR method translational symmetry is used and the appropriate Green's functions are Fourier transformed to k space. It is therefore a natural starting point for comparing electronic-structure calculation techniques and the multiple-scattering theories used in near-edge structure analysis. The LKKR method[16,17] is an outgrowth of theoretical work on low-energy electron diffraction (LEED).[21,22] The material is first divided into layers. Multiple scattering within the layers is solved with a partial-wave basis, while multiple scattering between the layers is solved within a plane-wave basis. Using layer doubling and layer stacking, the full infinite structure can be assembled in a manner that only requires two-dimensional translational symmetry. The time to complete this calculation is proportional to the number of layers; thus for systems with a complexity in the layer stacking sequence such as grain boundaries, surfaces, and multilayer bulk materials are ideal structures for the LKKR method. The ability of the LKKR method to handle grain boundary structures is important given the interest in possible changes in electronic structure arising from impurity segregation and the corresponding effects on the mechanical properties. Calculations can also help in the interpretation of electron-energy-loss spectroscopy (EELS) measurements of these changes at high spatial resolution in the scanning transmission electron microscope.

In this paper we use MgO as a test case to compare near-edge structure calculated using the LKKR method, XANES, and FEFF. It is particularly convenient because the spectroscopic fine structures can be easily understood on the basis of a simple physical model. We go on to show how the LKKR method can also give good agreement with the NES on the O K edge in rutile. This is particularly significant as the first two peaks have been interpreted as transitions to unfilled molecular orbital states that might not be modeled correctly by a simple superposition of atomic potentials. We also successfully apply the LKKR method to the calculation of near-edge structure in copper and show that the method can be used with confidence to explore changes due to alloying and impurity segregation. Finally, we discuss some of the limitations of such an approach. It would appear that the assumption of flat interstitial regions and the neglect of nonspherical contributions to the potential are more serious in loosely packed compounds than the neglect of core-hole effects.

THEORY

An extensive description of the LKKR method has been published previously.[16,17] Here we review only those features that are necessary to understand the relationship of LKKR to Green's-function-based multiple-scattering theories of NES. We aim to calculate the x-ray-absorption or electron-energy-loss spectrum in the dipole approximation. The transition rate for x-ray absorption is given in atomic units by

$$W_c(E) = -2 \int dr' \int dr \; \phi_c^*(r') \Delta^*(r') \, \mathrm{Im} G^+(r', r, E) \Delta(r) \phi_c(r), \tag{1}$$

where

$$\Delta(\mathbf{r}) = iA(\mathbf{r}) \cdot \boldsymbol{\nabla} \tag{2}$$

is the perturbation due to the incident x rays of angular frequency ω and magnetic vector potential $A(\mathbf{r})$. In the above expressions c is the speed of light, E the energy of the ejected electron, ε_c that of the core electron, ϕ_c the wave function of the core state, G^+ the retarded Green's function of the excited electron, and $\mathbf{r}$ and $\mathbf{r}'$ are position vectors. For EELS the $\Delta(r)$ would be replaced by $\exp(i\mathbf{q}\cdot\mathbf{r})$,[23] which would be approximated by $\mathbf{q}\cdot\mathbf{r}$ under dipole scattering conditions.[24–26]

The Green's function $G^+(E)$ may be written as

$$G^+(E) = \sum_n |n\rangle\langle n| (E + i\varepsilon - H)^- = \sum_n |n\rangle\langle n| (E + i\varepsilon - E_n)^-, \tag{3}$$

where H is the electronic Hamiltonian and $|n\rangle$ represents an eigenstate of H of eigenvalue E_n. Using Dirac's relation

$$\frac{1}{E - E_n + i\varepsilon} = \mathrm{P}\left(\frac{1}{E - E_n}\right) - i\pi\delta(E - E_n), \tag{4}$$

where P represents the principal part, we see that

$$\mathrm{Im}G^{+}(E)=-\pi\sum_{n}\delta(E-E_n)|n\rangle\langle n| \tag{5}$$

and

$$\begin{aligned}\mathrm{Im}G^{+}(r,r',E)&=-\pi\sum_{n}\delta(E-E_n)\langle r'|n\rangle\langle n|r\rangle\\&=-\pi\sum_{n}\delta(E-E_n)\psi(r',E_n)\psi^{*}(r,E_n)\\&=-\pi\rho(E)\Psi(r',E_n)\psi^{*}(r,E_n),\end{aligned} \tag{6}$$

where

$$\rho(E)=\sum_{n}\delta(E-E_n) \tag{7}$$

is the density of states at energy E. Substituting Eq. (6) into Eq. (1) yields

$$W_c(E)=2\pi\rho(E)|M(E)|^2. \tag{8}$$

$M(E)$ is the matrix element given by

$$M(E)=\int\Psi^{*}(r,E)\Delta(r)\phi_c(r)dr \tag{9}$$

for a transition from a core state $\phi_c(\mathbf{r})$ to the excited state $\psi(\mathbf{r},E)$. Equations (7)–(9) show that Eq. (1) is equivalent to Fermi's golden rule with Planck's constant $\hbar=1$ (a.u.). In the XANES program[2,3] the Green's function (3) is evaluated by calculating the scattering matrices of a set of spherical shells centered on the emitter. In the LKKR approach that is the subject of this paper, it is considered as the sum of an atomic contribution G_α from a particular site α and the contributions from the other atoms in the solid, i.e.,[16,17]

$$G=G^{\alpha_i}+(1+G_0t^{\alpha_i})(t^{\alpha_i})^{-1}(\tau^{\alpha_i\alpha_i}-t^{\alpha_i})(t^{\alpha_i})^{-1}(1+t^{\alpha_i}G_0), \tag{10}$$

where we drop the superscript + from the Green's function for simplicity, t^{α_i} is the isolated atomic scattering operator, and $\tau^{\alpha_i\beta_i}$ is the scattering path operator that includes all multiple-scattering events starting on site α and ending on site β in layer i. The atomic Green's function G^{α_i} is formed from regular and irregular numerical solutions to the Schrödinger equation for that particular atom. The difference between XANES and LKKR is the way in which the scattering path operator in Eq. (10) is evaluated.

In a LKKR calculation, the material is first partitioned into layers of atoms. For calculations involving surfaces or interfaces this division appears naturally from the problem. For bulk materials any convenient planes can be taken, though the calculation will be most efficient if the planes are densely packed low-index planes with reasonable interplanar spacings. Within the layers the atoms are represented by spherical muffin tins and Mattheiss's method[9] is used to combine the atomic charges to give the initial potential. This initial potential is identical to that used in the XANES theory. The interstitial potential between the muffin tins is assumed to have a constant value, which is a limitation compared to full potential methods such as the full-potential linear augmented plane-wave in which the interstitial potential is expanded as a Fourier series. This limitation might not be so serious for our application as we are only concerned with the densities of states inside the muffin-tin spheres projected out by the spatially localized inner-shell wave function. The scattering operator for layer i (T_i) is calculated using a two-dimensional form of KKR theory and is expressed solely in terms of an angular-momentum basis set as

$$[T_i^{-1}]_{LL'}^{\alpha_i\beta_i}=(t^{\alpha_i})^{-1}\delta_{\alpha_i\beta_i}\delta_{LL'}-G_{L\alpha_iL'\beta_i}. \tag{11}$$

L and L' refer to the angular momenta and $G_{L\alpha_iL'\beta_i}$ is the two-dimensional lattice Fourier transform of the Bloch free-space Green's function. The scattering from the individual atoms is calculated from phase shifts evaluated at the muffin-tin radii from the logarithmic derivative of the wave functions in the usual manner.

Scattering matrices representing transmission from left to right, T^{++}; right to left, T^{--}; reflection on the left-hand side, T^{-+}; and reflection on the right-hand side, T^{+-}; can now be constructed using LEED theory. A scattering operator for a bulk crystal can be assembled by successively adding layers to form the scattering matrices for a half space. The effect of more distant layers becomes progressively smaller and the process converges. The site diagonal scattering path operator for an atom in layer i needed in the evaluation of the Green's function can be written as

$$\tau^{\alpha_i\alpha_i}=\int dk(t^{-1}-G-\Delta)^{-1}_{\alpha_i\alpha_i}, \tag{12}$$

where Δ describes the embedding of layer i in the host crystal. The matrix Δ is found from the scattering matrices of the left (R^{-+}) and right (R^{+-}) half spaces that, once layer i is inserted, form the infinite crystal:

$$\Delta=(1+R^{+-})(1-R^{-+}R^{+-})(1+R^{-+})-1. \tag{13}$$

The problem of an interface region embedded between two semi-infinite bulk crystals is treated in the same manner.

In the XANES method the region around the excited atom is divided into concentric shells. This is fairly straightforward in simple high-symmetry materials, but the division becomes less useful for low-symmetry or disordered systems. Scattering operators are assembled for each shell and then scattering between shells is evaluated using operators for transmission across a shell (inward or outward) and reflection between shells. The boundary condition on the outermost shell requires that there is only an outgoing spherical wave. Topologically this process is identical to that used for LKKR except that the planar geometry has been changed to a spherical geometry.

In the LKKR code self-consistency is achieved by calculating a new potential from the charge density. Exchange and correlation contributions are found using the local-spin-density approximation and the Coulomb potential from a solution to the Poisson equation. The latter includes the long-range Madelung term. The potential used as input to the next iteration is found using Broyden's method,[27] which uses values from many previous iterations. Iterations are continued until convergence is achieved.

The density of states is then evaluated using Eq. (5). In practice the Green's function is evaluated at an energy offset

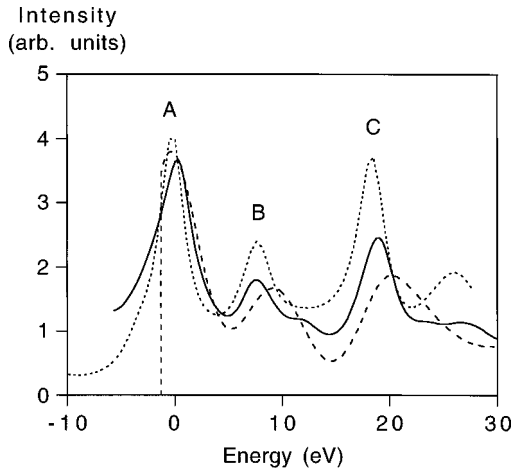

FIG. 1. LKKR (solid line), XANES (short-dashed line), and FEFF (long-dashed line) calculations for the MgO oxygen *K*-edge near-edge structure.

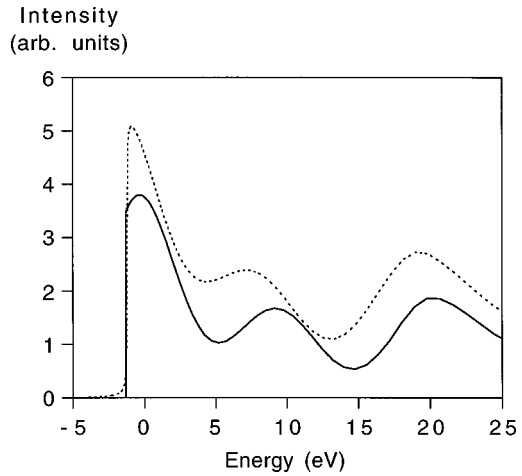

FIG. 2. FEFF calculations for the MgO oxygen *K*-edge near-edge structure with $r_{max}=12.0$ Å (solid line) and $r_{max}=6$ Å (dashed line).

by a small imaginary part δ to improve convergence. This is equivalent to broadening the density of states by a Lorentzian of width δ and can be used to simulate the effects of lifetime and instrumental broadening. In the calculations reported here a width of 0.005 hartree (0.0136 eV) was used. The densities of states were multiplied by the square of matrix elements calculated from wave functions generated using the Hartree-Slater potential of Herman and Skillman[28] in order to produce appropriate spectra.[29]

RESULTS AND DISCUSSION

The near-edge structure on both the oxygen and magnesium *K* edges of MgO has been extensively studied. The oxygen *K* edge represents a good test case as the characteristic three-peak structure shown in calculations of Fig. 1 has a simple physical explanation.[30] An oxygen atom is surrounded by a first coordination shell of magnesium atoms. The second coordination shell is oxygen and subsequent coordination shells alternate between magnesium and oxygen. A similar picture applies for magnesium, except of course that the first coordination shell is oxygen. Scattering from oxygen atoms dominates in MgO and to a good approximation scattering from magnesium can be neglected. The third peak, peak *C*, is a single-scattering EXAFS peak from the second coordination shell (first oxygen shell). The second peak labeled *B* is probably a single-scattering EXAFS peak from the fourth coordination shell (second oxygen shell), though it is affected to some degree by double scattering with the second coordination shell. The large peak *A*, just after the threshold, arises from an intrashell triangular scattering path in the second coordination shell (first oxygen shell). In Fig. 1 XANES, LKKR, and FEFF calculations for the oxygen *K* edge are compared. In all cases the magnesium muffin-tin radius was taken as 2.17 a.u. and the oxygen muffin-tin radius was 1.8 a.u. All the main peaks have the same relative height and are in the same position. An extra peak *B*2 appears in the LKKR calculation above the main peak *B*. Presumably this arises from the longer effective scattering paths considered in the LKKR calculation. Note that the peaks are broader in the FEFF calculation. This might be because FEFF does not adequately sum over many paths whose individual contributions are quite small. To demonstrate this effect we show in Fig. 2 a comparison between a FEFF calculation with a maximum path length r_{max} of 6 Å and another calculation where r_{max} has been increased to 12 Å. Increasing the maximum path length allows for more scatterings and narrows the peaks, which clearly shows the importance of multiple intershell scattering. Multiple constructive interference in this case is acting to sharpen the peaks as in a Fabry-Pérot interferometer.

Near-edge structure calculated using XANES, LKKR, and FEFF for the Mg *K* edge assuming no core hole are shown in Fig. 3. The calculations are all in good agreement with each other and experimental results. Note that all the peaks in the experiment are reproduced by the calculation, though the first two peaks labeled *A* and *B* have different relative heights. To investigate the magnitude of core-hole effects using FEFF, calculations both with and without a core hole are compared in Fig. 4. The core hole slightly shifts the energy of the high-energy peaks and redistributes intensity between peaks *A* and *B*. Significantly it does not create new

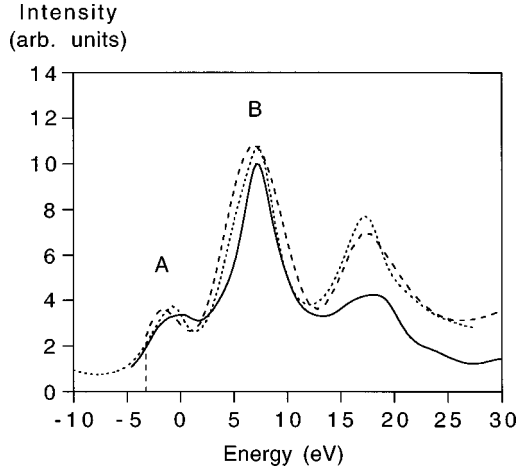

FIG. 3. LKKR (solid line), XANES (short-dashed line), and FEFF (long-dashed line) calculations for the MgO magnesium *K*-edge near-edge structure.

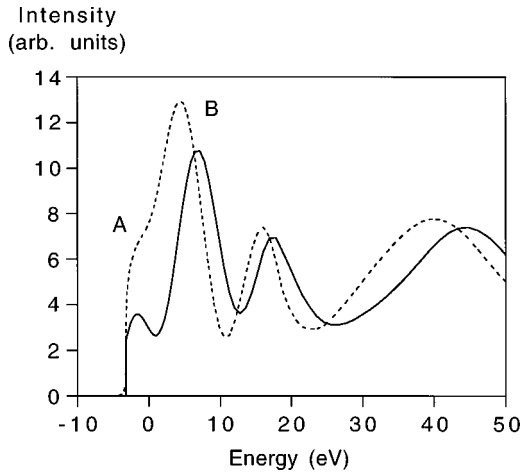

FIG. 4. FEFF calculations for the MgO magnesium K-edge near-edge structure with (dashed line) and without (solid line) a core hole.

peaks, merely emphasizing the first peak while suppressing the second. A similar calculation for the oxygen K edge showed that the core hole had a minimal effect. This is not surprising as core holes are expected to be more important at cation edges as shown in calculations for transition-metal oxides.[31]

The oxygen K edge in magnesium oxide represents a case where the filled valence band is made up from O $2p$ states and all transitions are to empty p-like states in the conduction band. It would not be surprising if methods such as XANES and FEFF, which make no attempt to calculate the ground-state electronic structure, did not successfully predict the features of the near-edge structure. Near-edge features that arise from transitions to empty states in a partially filled band may not be correctly modeled by a non-self-consistent multiple-scattering calculation that may successfully reproduce the higher-energy EXAFS peaks. The peaks at the threshold of the oxygen K edge from the rutile form of TiO_2 show transitions to the unfilled t_{2g} and e_g molecular orbitals. Figure 5 shows a comparison between a spectrum simulated using LKKR and our experimental EELS measurement. The

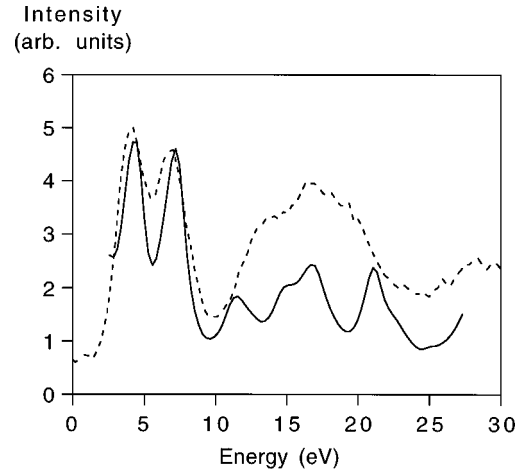

FIG. 5. LKKR calculation of the TiO_2 (rutile) oxygen K-edge near-edge structure (solid line) compared with the EELS experiment (dashed line).

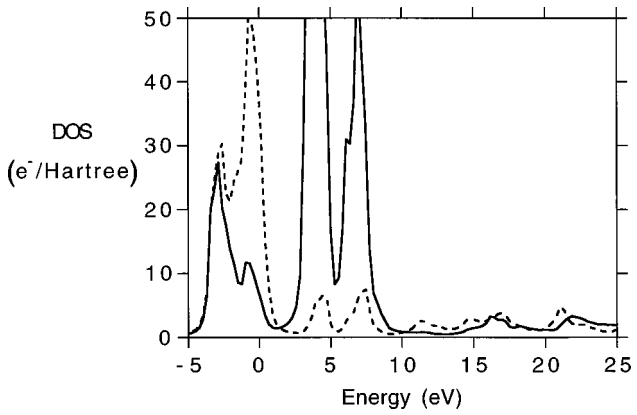

FIG. 6. Ti d density of states (solid line) in TiO_2 (rutile) compared with the O p density of states (dashed line).

LKKR calculation was based on the (001) layers and the muffin-tin radii were 1.9 a.u. for Ti and 1.7 a.u. for O. Not only does the LKKR calculation reproduce the t_{2g} and e_g peaks, but it also correctly shows the three-peak structure between 10 and 20 eV, which is best interpreted in a multiple-scattering framework. Earlier work[12] showed that this three-peak structure could be successfully simulated by the XANES program. The oxygen K edge in rutile is an interesting case because many calculations have succeeded in producing either transitions to unfilled molecular orbitals[32,33] or the extended fine structure[12,34] but never convincingly both sets of features. The LKKR method, as a true self-consistent electronic-structure code, will produce transitions related to electronic structure. As it is also a Green's-function method identical to the conventional multiple-scattering theories, it will have no problem with extended fine structures. The molecular-orbital splitting is also seen in Fig. 6, which shows the Ti d density of states.

The boron K edge from TiB_2 is shown as another example of near-edge structure in a titanium compound. TiB_2 is hexagonal with the structure shown in Fig. 7. For the calculation a muffin-tin radius of 2.4 a.u. was assumed for Ti and 2.1 a.u. for B with layers parallel to (0001). The near-edge structure at the boron K edge is compared with experiment in Fig. 8, again with very good agreement.

As mentioned above, the LKKR method is based on the muffin-tin approximation, which can be expected to cause problems in materials with highly directional bonding such as diamond or silicon. It is possible to calculate a band structure and total energy by filling the empty spaces at $\frac{1}{4},\frac{1}{4},\frac{3}{4}$ and $\frac{1}{2},0,0$ with empty spheres. It is also possible to use the space-

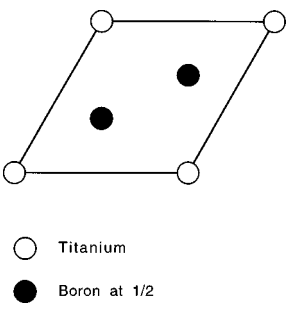

FIG. 7. Structure of TiB_2.

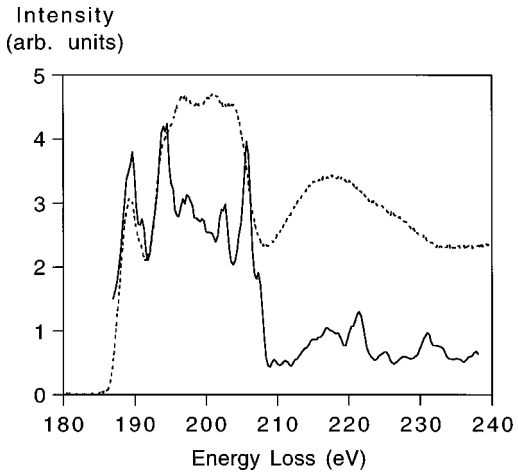

FIG. 8. LKKR calculation of the TiB_2 boron K-edge near-edge structure (solid line) compared with the EELS experiment (dashed line).

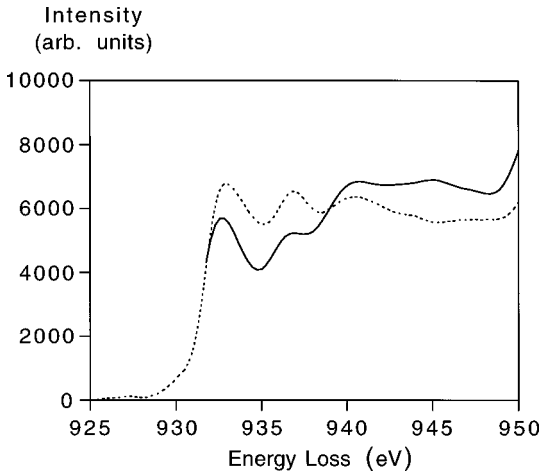

FIG. 10. LKKR calculation of the Cu L_3-edge near-edge structure (dashed line) compared with the EELS experiment (solid line).

filling atomic sphere approximation. In this case the interstitial region is removed by expanding the muffin-tin spheres to form overlapping space filling spheres. There is some similarity between the densities of states and the results of other calculations such as the linear augmented plane wave or pseudopotential, but the agreement with the K-shell fine structure in diamond (Fig. 9) is not as good as pseudo-atomic-orbital calculations.[35] A useful indicator of whether a calculation will be successful is the ratio of the volume in the muffin tins, assuming that they are just touching along the bond directions, to the total volume in the unit cell. Without the introduction of empty spheres for MgO this is 0.756, for rutile it is 0.33, for TiB_2 it is 0.566, and for silicon or diamond it is only 0.09. Inclusion of empty spheres can improve the packing fraction and the accuracy of the calculation provided high-symmetry sites suitable for placing empty spheres can be identified. The LKKR method would be expected to do well for closely packed metals where core-hole effects are negligible due to screening. This is indeed the case and as an example we show as Fig. 10 a calculation for the Cu L_3 edge compared with an experimental result. We have been extensively using the LKKR method to calculate unoccupied d densities of states observed in the L_{23} spectra from transition metals and these results will be reported elsewhere.

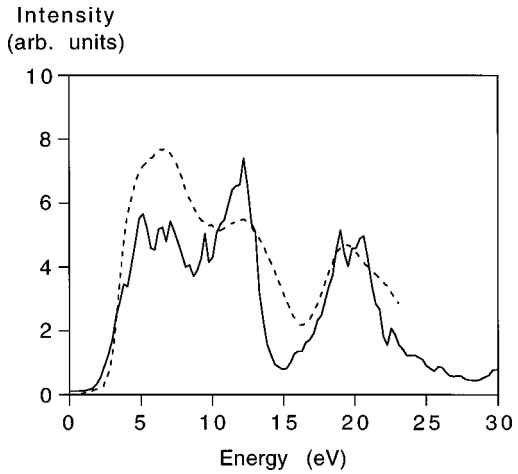

FIG. 9. LKKR calculation of the carbon K edge in diamond (solid line) compared with the EELS experiment (dashed line).

CONCLUSIONS

Multiple-scattering Green's-function theories can successfully be used to calculate near-edge structure at higher energies above threshold than those features that would be interpreted as transitions to partially filled states. Even though a relatively small number of simple single-scattering and triangular double-scattering paths can be used to explain the position of near-edge structure peaks, interference from multiple intershell scattering can substantially narrow these features.

To explain the details of the fine structure closer to threshold, in cases involving transitions to molecular orbitals or partially filled bands, it is absolutely essential to calculate the densities of states using a self-consistent potential. The LKKR method provides a convenient Green's-function method for calculating partial densities of states needed to interpret inner-shell fine structure. Since it is based on the same Green's-function expression as the multiple-scattering theories of near-edge structure, it will also reproduce the extended fine structures 50–100 eV above an edge. In particular it is exceptionally well suited to problems encountered in high-spatial-resolution EELS where inner-shell spectroscopic fine structure is measured at boundaries and interfaces. We have shown that the LKKR method successfully reproduces the fine structure in a number of materials, including both insulators and metals. Results for the oxygen K edge in rutile show that it can successfully simulate both the transitions to molecular orbitals and the extended fine structures.

The LKKR method is an electronic-structure technique for bulk materials, surfaces, and interfaces. As such it does not take account of core-hole effects, though in principle it would be possible to perform a calculation in which the excited atom is treated separately in its own layer. The calculation would then resemble an interface calculation. The lack of a self-consistent charge density is not intrinsic to the other multiple-scattering theories. Such a feature could be incorporated in the existing multiple-scattering codes with some effort.

The most serious restrictions to the application of LKKR will be in loosely packed materials with highly directional bonds, which cannot easily be decomposed into atomic spheres or muffin tins with a constant interstitial potential. We feel that if the material is divided into muffin tins that touch along the interatomic bonds, then the ratio of volume in the muffin tins to the total cell volume is a useful indicator of whether a LKKR calculation will successfully simulate near-edge structure. If high-symmetry sites suitable for placing empty spheres could be identified in the crystal, then the packing fraction and the accuracy of the calculation could be improved.

ACKNOWLEDGMENTS

We would like to thank Dr. L. A. J. Garvie, Dr. P. Fallon, and V. J. Keast for providing experimental spectra and the NSF for financial support through Grant No. DMR 930-6253. J.M.M. acknowledges the support of a DOE-EPSCOR cluster grant and DOE-LEQSF Grant No. (1993-95)-03. D.K.S. is grateful to the NSF for Grant No. DMR 930-0275.

[1] E. A. Stern, Phys. Rev. B **10**, 3027 (1974).
[2] P. J. Durham, J. B. Pendry, and C. H. Hodges, Comput. Phys. Commun. **25**, 193 (1982).
[3] D. D. Vvedensky, D. K. Saldin, and J. B. Pendry, Comput. Phys. Commun. **40**, 421 (1986).
[4] T. Fujikawa, T. Matsuura, and H. Kuroda, J. Phys. Soc. Jpn. **52**, 905 (1983).
[5] T. Fujikawa, J. Phys. Soc. Jpn. **57**, 306 (1988).
[6] S. I. Zabinsky, J. J. Rehr, A. Ankudinov, R. C. Albers, and M. J. Eller, Phys. Rev. B **52**, 2995 (1995).
[7] C. R. Natoli, M. Benfatto, and S. Doniach, Phys. Rev. A **34**, 4682 (1986).
[8] C. R. Natoli, M. Benfatto, C. Brouder, M. F. Ruiz Lopez, and D. L. Foulis, Phys. Rev. B **42**, 1944 (1990).
[9] L. F. Mattheiss, Phys. Rev. A **133**, 1399 (1964).
[10] V. L. Shneerson, W. T. Tysoe, and D. K. Saldin, Phys. Rev. B **53**, 10 177 (1996).
[11] J. E. Muller and J. W. Willkins, Phys. Rev. B **29**, 4331 (1984).
[12] P. Rez, J. Bruley, P. Brohan, M. Payne, and L. A. J. Garvie, Ultramicroscopy **59**, 159 (1995).
[13] T. J. Loucks, *The Augmented Plane Wave Method* (Benjamin, New York, 1967).
[14] J. Korringa, Physica (Amsterdam) **13**, 392 (1947).
[15] W. Kohn and N. Rostoker, Phys. Rev. **94**, 1111 (1954).
[16] J. M. Maclaren, S. Crampin, D. Vvedensky, and J. B. Pendry, Phys. Rev. B **40**, 12 164 (1989).
[17] J. M. Maclaren, S. Crampin, and D. Vvedensky, Phys. Rev. B**40**, 12 176 (1989).
[18] J. Mustre de Leon, J. J. Rehr, S. I. Zabinsky, and R. C. Albers, Phys. Rev. B **44**, 4146 (1991).
[19] V. L. Shneerson, W. T. Tysoe, and D. K. Saldin, Phys. Rev. B **51**, 13 015 (1995).
[20] P. J. Braspenning, R. Zeller, A. Lodder, and P. H. Dederichs, Phys. Rev. B **39**, 6334 (1989).
[21] J. B. Pendry, *Low Energy Electron Diffraction* (Academic, London, 1974).
[22] M. A. Van Hove, W. H. Weinberg, and C.-M. Chan, *Low Energy Electron Diffraction* (Springer, Berlin, 1986).
[23] R. F. Egerton, *Electron Energy Loss Spectroscopy in the Electron Microscope* (Plenum, New York, 1986).
[24] J. J. Ritsko, S. E. Schnatterly, and P. C. Gibbons, Phys. Rev. Lett. **32**, 671 (1974).
[25] D. K. Saldin and J. M. Yao, Phys. Rev. B **41**, 52 (1990).
[26] D. K. Saldin and Y. Ueda, Phys. Rev. B **46**, 5100 (1992).
[27] D. D. Johnson, Phys. Rev. B **38**, 12 807 (1988).
[28] F. Herman and S. Skillman, *Atomic Structure Calculations* (Prentice-Hall, Englewood Cliffs, NJ, 1963).
[29] R. D. Leapman, P. Rez, and D. F. Mayers, J. Chem. Phys. **72**, 1232 (1980).
[30] P. Rez, X. Weng, and H. Ma, Microsc. Microanal. Microstruct. **2**, 143 (1991).
[31] F. M. F. de Groot, M. Grioni, J. C. Fuggle, J. Ghijsen, G. A. Sawatzky, and H. Petersen, Phys. Rev. B **40**, 5715 (1989).
[32] J. A. Tossell, D. J. Vaughan, and K. H. Johnson, Am. Mineral. **59**, 319 (1974).
[33] T. A. Sasaki and T. Soga, Physica B **111**, 304 (1981).
[34] R. Brydson, H. Sauer, W. Engel, J. M. Thomas, E. Zeitler, N. Kosugi, and H. Kuroda, J. Phys. Condens. Matter **1**, 797 (1989).
[35] X. Weng, P. Rez, and O. F. Sankey, Phys. Rev. B **40**, 5694 (1989).